An experimental-numerical investigation on the effects of macroporous scaffold geometry on cell culture parameters

Hadis Eghbali[1], Michele M. Nava[2], Gabriella Leonardi[2], Davod Mohebbi-Kalhori[1], Roberto Sebastiano[2], Abdolreza Samimi[1], Manuela T. Raimondi[2]

[1] Department of Chemical Engineering, University of Sistan and Baluchestan, Zahedan - Iran
[2] Giulio Natta Department of Chemistry, Materials and Chemical Engineering, Politecnico di Milano, Milan - Italy

ABSTRACT

Introduction: Perfused bioreactors have been demonstrated to be effective in the delivery of nutrients and in the removal of waste products to and from the interior of cell-populated three-dimensional scaffolds. In this paper, a perfused bioreactor hosting a macroporous scaffold provided with a channel is used to investigate transport phenomena and culture parameters on cell growth.
Methods: MG63 human osteosarcoma cells were seeded on macroporous poly(ε-caprolactone) scaffolds provided with a channel. The scaffolds were cultured in a perfused bioreactor and in static conditions for 5 days. Cell viability and growth were assessed while the concentration of oxygen, glucose and lactate were measured. An in silico, multiphysics, numerical model was set up to study the fluid dynamics and the mass transport of the nutrients in the perfused bioreactor hosting different scaffold geometries.
Results: The experimental and numerical results indicated that the specific cell metabolic activity in scaffolds cultured under perfusion was 30% greater than scaffolds cultured under static conditions. In addition, the scaffold provided with a channel enabled the shear stress to be controlled, the initial seeding density to be retained, and adequate mass transport and waste removal.
Conclusions: We show that the macroporous scaffold provided with a channel cultured in a macroscale bioreactor can be a robust reference experimental model system to systematically investigate and assess crucial culture parameters. We also show that such an experimental model system can be employed as a simplified "representative unit" to improve the performance of both perfused culture systems and hollow, fiber-integrated scaffolds for large-scale tissue engineering.

Keywords: Macroporous scaffold, Perfused bioreactor, Poly(ε-caprolactone), Shear stress

Introduction

A basic concept in the design of dynamic culture systems for in vitro tissue engineering is to mimic the physiological microenvironment in which cells reside, providing the proper biochemical and biophysical stimuli (1, 2). Perfused bioreactors have been demonstrated to be effective in the delivery of oxygen and nutrients, and in the removal of waste products to and from the interior of three-dimensional (3-D) scaffolds (3, 4).

Scaffolds with macro and high interconnectivity pores have a prevascularization potential (4, 5). However, there are limitations when such scaffolds are used in a perfusion system, including cell washout (i.e., cell detachment) due to the hydrodynamic shear stress and the pressure drop within and across the scaffold, respectively, in short-term culture (6-9). Conversely, in mid-to-long-term culture, the accumulation of cells and extracellular matrix (ECM) in macroporous scaffolds results in a decrease of the scaffold porosity, affecting the delivery of nutrients, the removal of waste, the fluid flow distribution, and the local fluid shear stress, whose effect might be harmful for cell viability (2, 10, 11).

Several strategies have been adopted to prevent cell detachment and washout, including the functionalization of the scaffold surface by means of adhesive ligands (12). Alternatively, physical methods (13, 14), such as electric current (14), the creation of nano-sized pore scaffolds (15) and hollow fibers embedded in macroporous scaffolds (16, 17) have been used. In hollow-fiber bioreactor systems, which have been developed primarily as models to engineer vascularized,
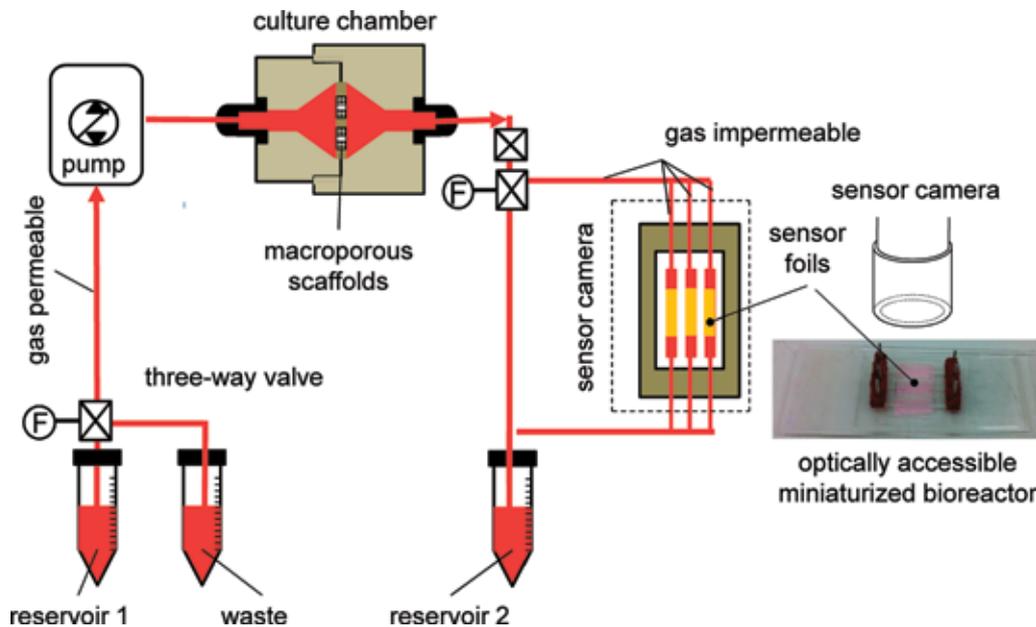
Fig. 1 - The perfused bioreactor experimental setup. The culture medium in reservoir 1 flows through gas permeable tubes to the culture chamber and to the reservoir 2. The culture chamber may hold 3 scaffolds. At the outlet of the culture chamber, a by-pass circuit composed of a 3-way valve and a gas-impermeable tubing with an optically accessible miniaturized bioreactor allows the oxygen concentration in the culture medium to be measured. The exhausted culture medium in reservoir 2 was reversed and collected in a waste reservoir to assess glucose and lactate content.

critical-size tissues (i.e., greater than millimeters), the medium flows through fibers, preventing cells from being directly exposed to hydrodynamic shear. Thus, cell detachment can be prevented, while the transport of nutrients, as well as the removal of waste metabolites, occur by convection at the fiber interface and by diffusion beyond the fiber wall (3). However, the control of critical culture parameters in these macroscopic dynamic culture systems is still a significant issue. In particular, the cell seeding density, their viability and their nonhomogenous cell distribution in a 3-D scaffold matrix affect the development and maturation of the functional tissue constructs (18, 19). For example, a low initial cell density has been demonstrated to negatively affect the formation of a mature mineralized bone (20) and a functional cartilage tissue (21).

Here, we propose an experimental-numerical model consisting of a perfused bioreactor to culture a cell-populated macroporous scaffold provided with a channel in its center. A channel of this sort may be considered the equivalent of a hollow fiber integrated into a macroporous scaffold. Our scaffold that reasonably allows the majority of the culture medium to flow through it, making it possible to reduce the pressure drop across the scaffold, to decrease the hydrodynamic shear stress acting on cells in short- and mid-to-long-term culture and, therefore, cell detachment. Indeed, it has been reported that in 3-D scaffolds, the critical shear stress causing detachment was from 2 to 4 orders of magnitude below the one measured in 2-D experiments (i.e., 1 Pa) (10, 22-24). On the other hand, a lower fraction of the culture medium may also flow through the scaffold pores that offer a greater resistance with respect to the central channel. Consequently, cells on the scaffold fibers and pores can be directly exposed to the fluid flow and relevant hydrodynamic shear stress. Furthermore, nutrient and waste removal can be greatly enhanced by convection and diffusion occurring in the interstitial perfused part of the porous scaffold.

In this work, we show that the macroporous scaffold provided with a channel cultured in a macroscale bioreactor can be a robust reference experimental model system for systematically investigating and assessing crucial culture parameters (i.e., oxygen, glucose, lactate) in a strictly controlled way, enabling straightforward numerical simulations. In addition, we show that such an experimental model system can be employed as a simplified "representative unit" or as a "representative domain" to improve the performance of both perfused culture systems and hollow fiber-integrated scaffolds for large-scale tissue engineering, overcoming their technological and practical limitations.

Materials and methods

The bioreactor design

The perfused bioreactor in this work was adapted from a previous study (7). It consists of a chamber connected by gas-permeable silicon tubing to 2 medium reservoirs. The priming volume of the circuit is 10 mL. A peristaltic pump (Watson-Marlow Bredel) maintains a constant flow rate (Q = 0.2 mL min^{-1}) to the cellularized construct located in the culture chamber (Fig. 1). The culture chamber carries 3 identically sized constructs, shaped as channeled discs (1-mm thick and 3.5 mm in radius, R_e) (Fig. 2).

To measure the oxygen concentration at the outlet of the culture chamber, a bypass circuit composed of a 3-way valve (located at the outlet culture chamber) and a gas-impermeable tube connected to an optically accessible miniaturized bioreactor (9) (Fig. 1) was introduced. The miniaturized bioreactor was equipped with oxygen sensor foils used for oxygen imaging (SF-RPSu4; PreSens) and a camera unit. The miniaturized bioreactor held 3 independent culture chambers equipped with oxygen sensor foils fitting the individual culture chamber (6 × 3 mm). Figure 1 shows the perfusion circuit used to assess the local
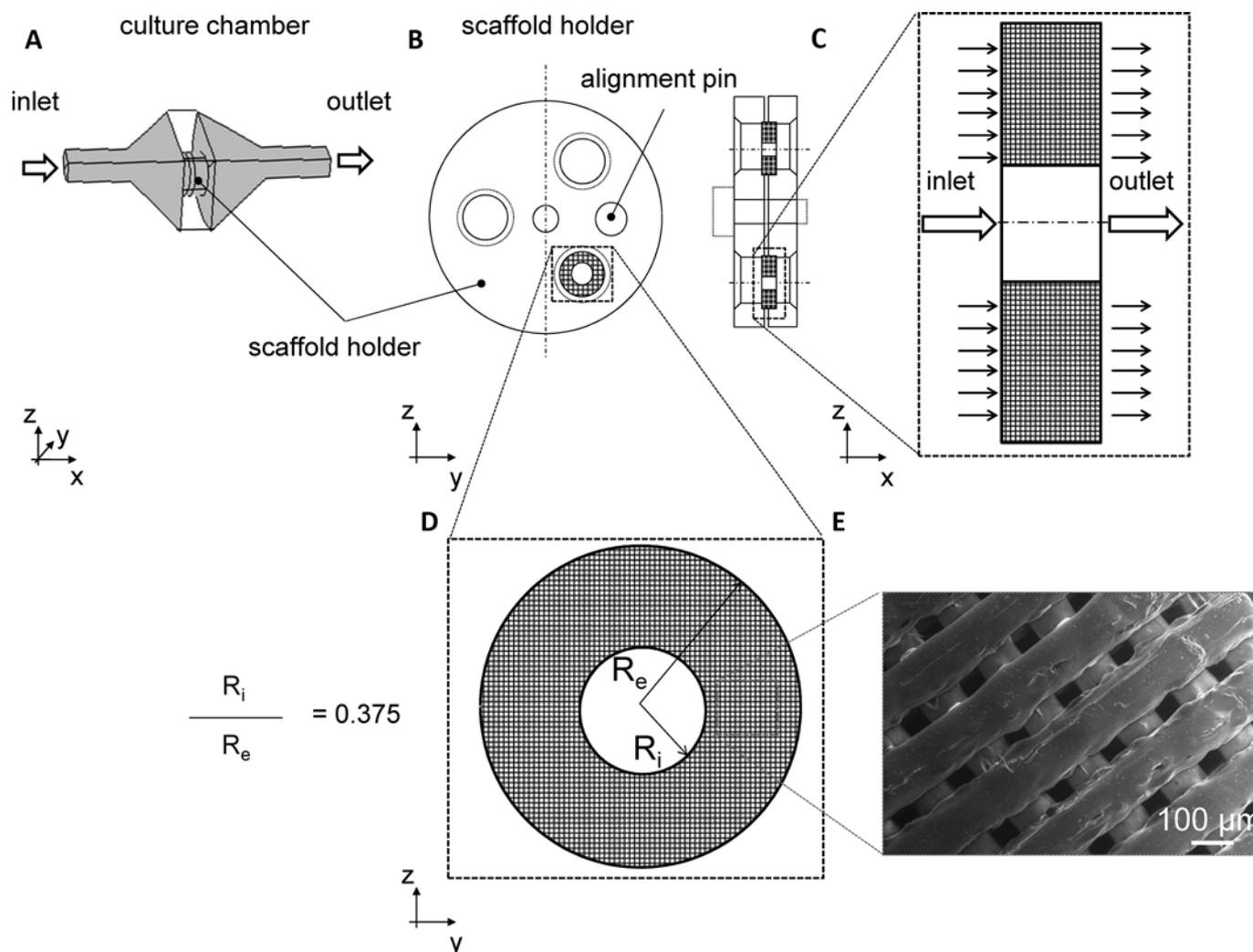
Fig. 2 - (A) CAD geometry of the culture chamber. **(B)** Scaffold position in the holder. **(C)** Lateral view of the scaffold holder. Zoomed view of the PCL scaffold. **(D)** Front view of the PCL scaffold with internal radius, R_i and external radius R_e. **(E)** SEM of the PCL scaffold.

oxygen concentration after a single passage of the medium flow.

To measure the glucose and lactate concentration deriving from the cell metabolism, a third reservoir (Fig. 1) (referred to as "waste") was introduced. After a single passage of the culture medium through the constructs, the culture medium flow was reversed and the exhausted culture medium (i.e., from reservoir 2) was collected in a waste reservoir for analysis by high-performance liquid chromatography (HPLC). The exhausted medium was sampled every 2 days. To prevent mixing the fresh and exhausted culture mediums, a 3-way valve was employed in the circuit to assess the glucose and lactate concentrations.

Cell preparation and scaffold seeding

Cells of the MG63 human osteosarcoma cell line (86051601-1VL; Sigma-Aldrich) were resuscitated and expanded in minimum essential medium (MEM) supplemented with 2 mM glutamine, 10% fetal calf serum (FCS), 1% nonessential amino acids (NEAAs), and 1% penicillin/streptomycin, under 5% CO_2 atmosphere at 37°C.

Poly(ε-caprolactone) (PCL) scaffolds manufactured by an additive biomanufacturing system, known as BioExtruders, was used (8, 25). The scaffolds were sterile discs, 1 mm in thickness and 3.5 mm in radius, with a mean pore diameter of 100 μm and an average porosity of 80%. Three constructs in parallel were placed in a holder (Fig. 2B-E). The discs were perforated using a precision die cutter in order to get an outer-inner radius ratio (R_i/R_e) equal to 0.375 (Fig. 2C, D). We chose R_i/R_e = 0.375 because this ratio is typically employed in the design of hollow-fiber scaffolds to ensure (diffusive) transport of nutrients to the cells residing in compartments surrounding the channel through which the culture medium flows (3). To increase the adhesion properties of the scaffold surface, the scaffolds were positioned in ultra-low adhesion, 24-well culture dishes (Costar 3473; Corning), wetted in a complete medium to obtain adhesion of serum proteins and, then dried after 3 hours. For the cell seeding, expanded cells were detached by trypsin, manually counted and seeded at a

volumetric cell density of approximately 7.5×10^4 cells/mm^3. Constructs were then incubated overnight at 37°C for cell adhesion. These cellularized scaffolds were transferred in the culture chamber at day 0, followed by the assembly of the bioreactor. At days 1, 3, and 5, the bioreactor was disassembled and assays were performed. Cell-populated scaffolds were also cultured in static conditions in ultra-low adhesion, 24-well culture dishes with medium replaced every 2 days. The exhausted medium for scaffolds cultured under static conditions was collected for HPLC analysis.

Cell morphology, viability, and number

To assess cell morphology, scaffolds were imaged at each time point by the scanning electron microscopy (SEM). The cell-populated scaffolds were fixed in the wells in 1.5% glutaraldehyde and 0.1 M sodium cacodylate, dehydrated in a graded series of ethanol. Then, the samples were air dried, glued onto SEM stubs, and gold-coated in a vacuum ion coater. All observations were carried out at 17.5 kV using a scanning electron microscope (EVO 50 EP; Carl Zeiss).

To assess cell viability, cellularized scaffolds were assayed for cell metabolic activity by Resazurin assay. In this assay, mitochondrial, cytosolic, and microsomal enzymes in viable cells reduce Resazurin into a fluorescent product (i.e., Resorufin). Conversely, nonviable cells rapidly lose their metabolic capacity, do not reduce the indicator dye and, thus, do not generate a detectable fluorescent signal. Briefly, a 0.2 mg/mL Resazurin (R7017; Sigma-Aldrich) solution was prepared in Dulbecco's phosphate buffered solution (PBS), sterilized by filtration and diluted 1:10 (v/v) with a cell culture medium. The culture medium was removed from the samples and replaced with 0.4 mL of Resazurin working solution. An empty well was also filled and used as a control. Scaffolds were incubated for 3.5 hours under standard conditions. The solution was then transferred to a 96-well cell culture plate, and its absorbance and fluorescence were measured by a spectrophotometer (Infinite M200 PRO; Tecan). Concerning the absorbance, the measurement and reference wavelengths were set to 570 and 600 nm, respectively. For the fluorescence measurements, the excitation wavelength was set at 560 nm and the emission wavelength was set at 590 nm (manual gain set to 60).

The DNA content was assessed on the cell lysate. The culture medium was replaced with deionized water and the culture plate containing the cellularized samples was frozen at -80 °C and incubated at 37°C repeatedly. The DNA absorbance was measured at 260 nm directly on the cell lysate with a spectrophotometer (Infinite M200 PRO; Tecan) equipped with a NanoQuant Plate.

Oxygen concentration assay

SF-RPSu4 oxygen sensor foils were used for oxygen imaging (PreSens). To assess the oxygen concentration in the perfused bioreactor, the sensor foils were cut into 6 × 3-mm rectangular pieces to fit the individual culture chambers (Fig. 1), while, for cellularized scaffolds cultured in static conditions, the sensor foil (7 × 7 mm) was located at the bottom of the culture well. The planar sensors consist of an oxygen

sensitive dye and a reference dye, which are immobilized in an oxygen-permeable polymer matrix and fixed on a transparent polyester layer (glossy side of the sensor) while a white oxygen transparent layer for optical isolation is turned towards the camera during measurement. The sensitive layer incorporates the fluorescent dyes and responds to oxygen. The dyes are immobilized within a polymer matrix that is highly permeable to oxygen. In this way oxygen can penetrate into the sensitive layer and interact with the fluorescent indicator dye while the dyes themselves cannot leach out (26).

In both culture conditions, the sensors were washed with distilled water, kept in 70% EtOH for 1 hour, dried, washed twice in cell culture-grade distilled water and kept wet in complete culture medium until use. In each experiment, images of the oxygen sensors were taken arbitrarily every 4 hours without interruption for 5 culture days. At each time step, each acquired image was converted into a map of local oxygen concentration by means of calibration parameters defining the 0% and 21% oxygen tension. These calibration values were determined according to our previous work (27). The 0% oxygen calibration value was determined by filling the culture chamber with 100% nitrogen and acquiring oxygen maps. The 21% oxygen calibration (corresponding to saturation) was determined by filling the incubator with fresh atmospheric air and acquiring oxygen maps. Once converted into local oxygen concentration values, the areas corresponding to the whole culture chamber surface were subdivided into 4 regions of interest and the mean oxygen concentration was calculated using the PreSens software.

To calculate the oxygen consumption rate of the cells in time, we applied a compartmental model of chemical consumption (27).

$$\overline{M}_{O_2} = Q(C_{O_{2IN}} - C_{O_{2OUT}}) \qquad \text{Eq. [1]}$$

where Q represents the experimental flow rate, $C_{O_{2IN}}$ and $C_{O_{2OUT}}$ are the average species concentration at the inlet $\left(C_{O_{2IN}} = 0.20\,mol/m^3\right)$ and measured at the outlet by means of the sensor foils, respectively. The oxygen consumption rate specific to cells M_{O_2}, was then calculated as follows (Eq. [2]):

$$M_{O_2} = \frac{\overline{M}_{O_2}}{N_V} \qquad \text{Eq. [2]}$$

where N_V is the cell density in the scaffold provided with a channel ($R_i/R_e = 0.375$) and $\overline{M}_{O_2}$ is the cell oxygen consumption calculated by Equation [1].

Glucose and lactate concentration assay via HPLC

The exhausted culture medium samples arising both from the perfusion bioreactor and the static culture were analyzed by HPLC using an Agilent/HP1100 Series system equipped with degasser unit, quaternary pump, autosampler, column thermostatic compartment, Agilent 1362A diode array

detector (DAD), Agilent 1315A refractive index detector (RID), ICSep ICE-ION-300 column, and ICSep ICE-ION-300 precolumn cartridge 2/pk by Transgenomic. Prior to sample analyses, the 3-KDa centrifugal filter units (Amicon Ultra-0.5) were washed and centrifuged at 14,100 rpm for 30 minutes twice with HPLC water. A volume of 1 mL of each sample was loaded into the washed filter and centrifuged at 14,100 rpm for 30 minutes. The filtered solution was then analyzed by HPLC under the following analysis conditions: column temperature 70°C, eluent H_2SO_4 0.0085 N solution, flow rate 0.4 mL/min, injection 100 μL. The glucose was monitored by DAD (r.t. = 15.7 min.) and lactic acid was monitored by DAD and RID (r.t. = 21.5 min). Data were acquired and processed by Agilent Chem Station software.

To calculate the glucose and lactate consumption and production rate of the cells in time, respectively, we applied the compartmental model of chemical consumption and relevant equations as follows (Eqs. [3a, b])

$$\overline{M}_{Glu} = Q(c_{GluIN} - c_{GluOUT}) \qquad \text{Eq. [3a]}$$

$$\overline{M}_{Lac} = Q(c_{LacOUT} - c_{LacIN}) \qquad \text{Eq. [3b]}$$

where Q represents the experimental flow rate, c_{GluIN}, c_{GluOUT} c_{LacIN} and c_{LacOUT} are the average species concentration at the inlet ($c_{GluIN} = 5.55 \ mol/m^3$, $c_{LacIN} = 0.00 \ mol/m^3$) and measured at the outlet, respectively. The glucose consumption and lactate production rates specific to cells M_{Glu} and M_{Lac} were then calculated as follows (Eqs. [4a, b]):

$$M_{Glu} = \frac{\overline{M}_{Glu}}{N_v}$$
$$\text{Eq. [4a]}$$

$$M_{Lac} = \frac{\overline{M}_{Lac}}{N_v}$$
$$\text{Eq. [4b]}$$

where N_v is the cell density in the scaffold provided with a channel ($R_i/R_e = 0.375$), $\overline{M}_{Glu}$ and $\overline{M}_{Lac}$ are the glucose consumption and lactate production calculated by Equations [3a] and [3b], respectively.

Computational fluid dynamics modeling

A multiphysics computational finite element model was developed to predict both the fluid dynamics quantities, including the average velocity and the hydrodynamic shear stress and the variation in oxygen and glucose concentration. We modeled one-third of the whole culture chamber (Fig. 3A, B), resulting in a cylindrical channel of radius $R_e = 3.5$ mm and of height H equal to 5 mm (Fig. 3D). In particular, we modeled the culture chamber holding 4 different scaffold geometries having different R_i/R_e, namely $R_i/R_e = 0.743$, $R_i/R_e = 0.375$ corresponding to the experimental model, $R_i/R_e = 0.185$ and $R_i/R_e = 0.000$, corresponding to the full

macroporous scaffold model (Fig. 3C). We chose these ratios because they are typically used in the design of hollow-fiber scaffolds to ensure (diffusive) transport of nutrients to the cells residing in compartments surrounding the channel through which the culture medium flows (3). The macroporous scaffold was composed of crossed fiber of 200 μm in diameter, resulting in a characteristic pore size of 100 μm and a porosity of 80%.

The medium fluid dynamics in the culture chamber were modeled by the Navier-Stokes equations for incompressible Newtonian fluids, namely by the continuity (Eq. [5]) and the momentum conservation equation (Eq. [6]), respectively

$$\nabla \cdot u = 0 \qquad \text{Eq. [5]}$$

$$\rho(u \cdot \nabla)u = \nabla \cdot \left(-pI + \mu(\nabla u + (\nabla u)^T)\right) + F \qquad \text{Eq. [6]}$$

where u is the velocity vector, ρ is the fluid density, p is the fluid pressure, μ is the dynamic viscosity of the fluid F and is the volume force vector. The hydrodynamic shear stress τ was calculated by Eqs. 7 and 8 (28):

$$\tau = \sqrt{\tau_{12}^2 + \tau_{23}^2 + \tau_{13}^2} \qquad \text{Eq. [7]}$$

$$\tau_{ij} = \mu\left(\frac{\partial u_i}{\partial x_j} + \frac{\partial u_j}{\partial x_i}\right) \qquad \text{Eq. [8]}$$

The mass transport equation in the fluid domain was modeled as follows (Eq. [9]):

$$u\nabla \cdot c_i - D_i \Delta c_i = 0 \qquad \text{Eq. [9]}$$

where c_i is the concentration of the i-species (for oxygen $i = O_2$ and glucose $i = Glu$), D_i is the diffusion coefficient of the i-species in the culture medium at 37°C and u is the fluid velocity predicted by Equations [5] and [6].

To account for cell growth and metabolic activity, the macroporous scaffold was modeled as follows (Eq. [10]):

$$\widetilde{M}_i + D_i \Delta c_i = 0 \qquad \text{Eq. [10]}$$

where $\widetilde{M}_i$ is the cell volumetric consumption rate that was assumed to be a function of the concentration of the i-species according to the Michaelis-Menten (M-M) kinetics.

$$\widetilde{M}_i = M_i \cdot \frac{c_i}{c_i + K_{m_i}} N_v \qquad \text{Eq. [11]}$$

M_i and K_{M_i} being the maximal consumption calculated from Eqs. 1- 4 and the M-M constant of the i-species (for oxygen $i = O_2$ and glucose $i = Glu$), respectively. The values imposed in the numerical analyses are gathered in Table I.

The geometry and the boundary conditions for the computational study are shown in Figure 3D. Concerning the fluid dynamics problem, one-third of the flow rate was imposed on the left surface of the modeled geometry, a null pressure at the right surface (i.e., outlet). No slip boundary conditions were imposed on either the inner surface of the
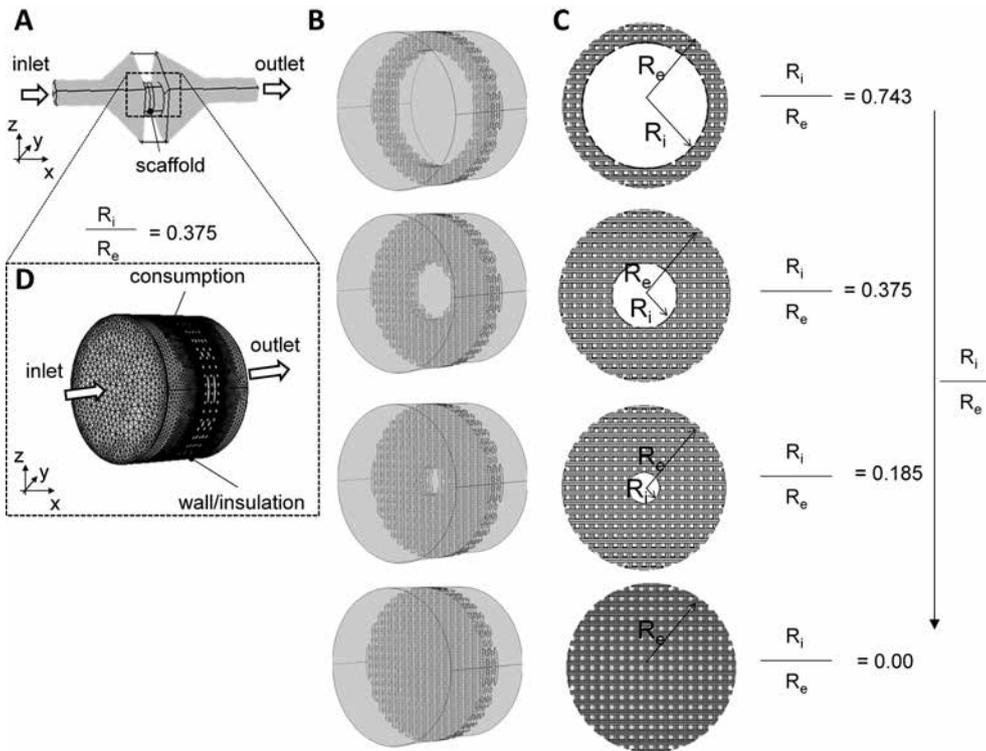
Fig. 3 - Computational model geometry and boundary conditions. (**A**) CAD geometry of the culture chamber. (**B**) Zoomed view of the culture chamber (one-third) holding the scaffold with decreasing R_i/R_e (**C**) CAD geometry of the scaffold with decreasing R_i/R_e (**D**) Meshed geometry of the culture chamber and boundary conditions. Numerical values are gathered in Table I.

TABLE I - Numerical values of the model parameters used in the numerical simulation

Symbol	Units	Description	Reference
H	5.00 mm	Culture chamber length	
L	1.00 mm	Scaffold thickness	
R_e	3.50 mm	Scaffold radius	
R_i	0.00 mm	Channel radius	This study
	0.65 mm		
	1.30 mm		
	2.60 mm		
Q	0.06 ml min^{-1}	Flow rate at the inlet	(7)
μ	8.10 10^{4-} Pa s	Fluid viscosity at 37°C	(1)
ρ	1000 kg m^{-3}	Fluid density at 37°C	(1)
D_{O_2}	2.00 10^{-9} m^{2}s^{-1}	Oxygen diffusion coefficient	(1)
D_{Glu}	9.59 10^{-10} m^{2}s^{-1}	Glucose diffusion coefficient	(34)
$K_{MM_{O_2}}$	0.15 mol m^{-3}	M-M constant for oxygen	(1)
$K_{MM_{Glu}}$	0.10 mol m^{-3}	M-M constant for glucose	(29)
$c_{O_{2IN}}$	0.20 mol m^{-3}	Inlet oxygen concentration	This study
$c_{Glu_{IN}}$	5.55 mol m^{-3}	Inlet glucose concentration	This study
M_{O_2}	2 μmol/h·10^6 cells	Oxygen consumption rate	This study
M_{Glu}	5 μmol/h·10^6 cells	Glucose consumption rate	This study
N_V	7.50·10^4 cells mm^{-3}	Cell density	This study

culture chamber or on the scaffold fibers. Regarding the mass transport model equations, a constant inlet concentration of both oxygen $c_{O,IN}$, and glucose c_{GluIN}, and the volumetric consumptions of both species $\widetilde{M}_i$, were imposed on the scaffold fibers.

The commercial software Comsol Multiphysics® (30) was used to set up, discretize, and solve the equations. The final mesh was composed of 5,000,000 of tetrahedral element. The numerical analyses were run on a Linux workstation with 32 Gb RAM.
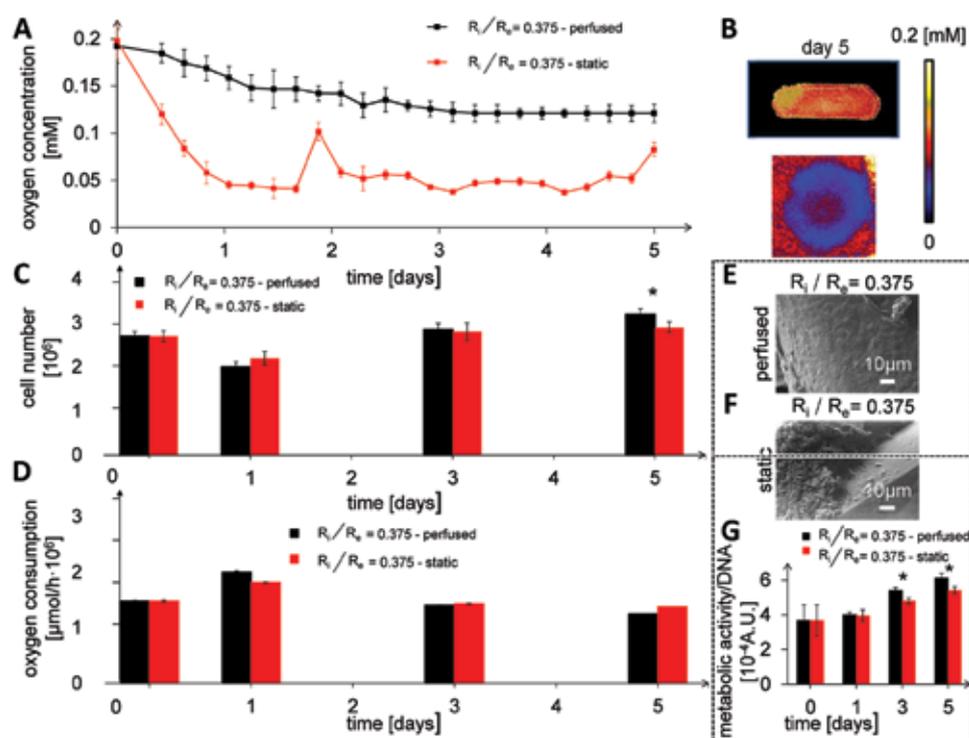
Fig. 4 - (A) Oxygen concentration profiles for scaffolds provided with a channel (R_i/R_e = 0.375) cultured in the perfused bioreactor and in static conditions. (B) Fluorescence pictures of the oxygen measurement in the perfused bioreactor and in the static controls taken at day 5. (C) Number of cells estimated in the scaffold provided with a channel (R_i/R_e = 0.375) cultured in the perfused bioreactor and under static conditions. (D) Oxygen consumption per million of cells estimated in the cell-populated scaffold provided with a channel (R_i/R_e = 0.375) cultured in the perfused bioreactor and under static conditions. (E) Results on cell morphology. SEM pictures of the PCL scaffolds (R_i/R_e = 0.375) cultured in perfused conditions. (F) Results on cell morphology. SEM pictures of the PCL scaffolds (R_i/R_e = 0.375) cultured under static conditions at day 5. (G) Cell metabolic activity normalized by the DNA content calculated by estimate in the cell-populated scaffold provided with a channel (R_i/R_e = 0.375) cultured under perfused and static conditions at days 0, 1, 3 and 5. *$p<0.01$.

Statistical analysis

Two experiments for each time point were performed, for a total of 6. Two experimental groups were compared: scaffold provided with a channel ($R_i/R_e = 0.375$) under perfusion and static conditions. Data were presented as mean and standard deviations. A nonparametric statistical analysis was performed by means of the Kruskall-Wallis followed by Mann-Whitney test. Differences were considered to be significant if p value <0.05.

Results and discussion

To assess cell morphology, cellularized scaffolds both in static and in the perfused bioreactor were imaged by SEM. As shown in Figure 4, cells subjected to a fluid flow adhered and spread well on the fibers in the perfused bioreactor (Fig. 4E). Conversely, the cellularized scaffolds cultured under static conditions showed a formation of aggregates due to the absence of the fluid flow (Fig. 4F).

To assess cell viability, the specific cell metabolic activity was calculated as the ratio between the fluorescence measurements and the DNA content at each time point. The cultured cells in the static conditions showed a comparable viability to the cells cultured in the perfused bioreactor at both days 0 and 1 (Fig. 4G) and the cell metabolic activity decreased about 2% from the initial value up to a significant increase both at days 3 and 5 (p value <0.01) if compared to the ones calculated for the scaffolds provided with a channel cultured under static conditions (Fig. 4G).

By comparison, in a previous study from our group in which chondrocytes were seeded on PCL macroporous scaffolds (i.e., no channel) and cultured in the perfused bioreactor described in Figure 1, the cell metabolic activity decreased by 60% to 73% in comparison to day 0 (7). This drop was likely due to a reduced cellularity caused by a partial washout of cells, as reported in the literature (11, 31, 32). In contrast, the scaffold provided with a channel ($R_i/R_e = 0.375$) enabled lower cell detachment during assembly and in operating conditions and led to higher cell viability because of the greater nutrient supply and waste removal to and from the cells.

To assess the oxygen consumption rate of the cells in time we measured the oxygen concentration (Figs. 4A, B) in the cell-populated scaffold provided with the channel ($R_i/R_e = 0.375$) cultured in perfusion and under static conditions. The oxygen tension decreased over time from 0.2 up to 0.14 mM after 5 days of culture, while a greater depletion of oxygen was measured on the cellularized scaffolds provided with the channel $R_i/R_e = 0.375$ cultured under static conditions (from 0.2 up to 0.05 mM on average) (Figs. 4A, B). These hypoxic conditions were maintained for the duration of the culture process, despite periodical changes of the medium.

Then, we estimated cell proliferation during culture time (Fig. 4C). At day 1, a reduction of cells in the scaffold provided with a channel ($R_i/R_e = 0.375$) cultured both with perfusion and under static conditions occurred (26% and 19%, respectively). Conversely, cell expansion was evident from day 1 to day 5 of perfusion (40%), whereas the number of cells increased 24% under static conditions. Given a certain cell density per scaffold and the previously determined oxygen concentration, we were able to calculate the average oxygen consumption of cells by means of Equations [1] and [2]. The results over a 5-day culture time are illustrated in Figure 4D. The calculated values ranged from approximately 1.25 to 2.00 μmol/h·10⁶ cells, which is 1 order of magnitude greater
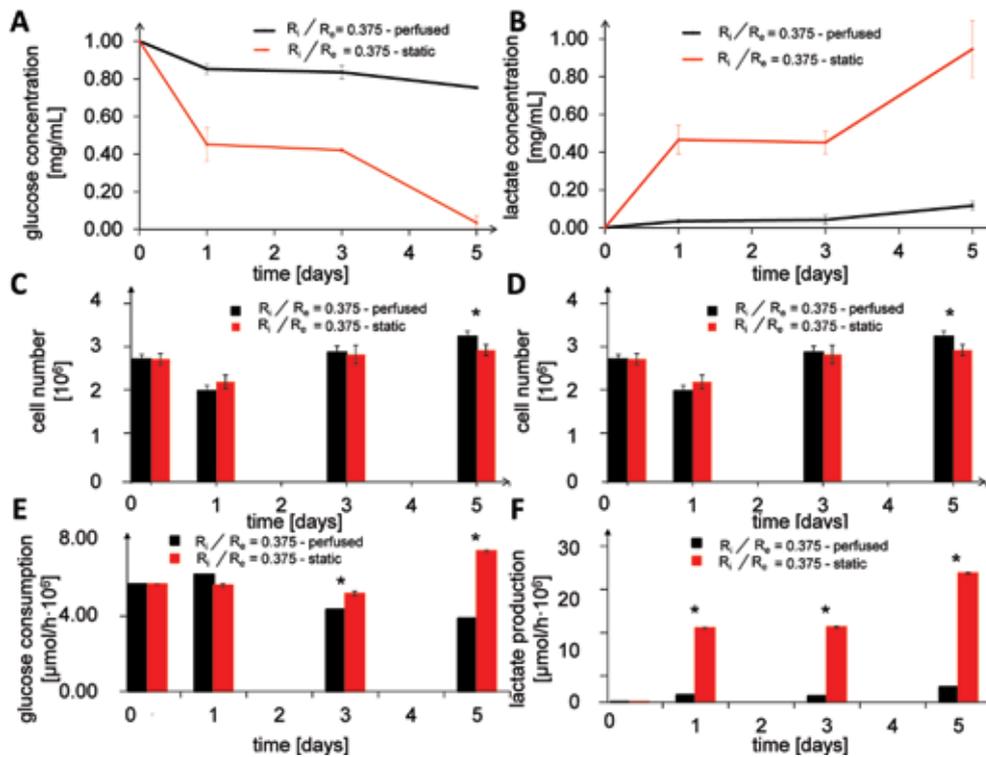
Fig. 5 - Results of the chemical analysis. (**A**) Glucose concentration profiles for scaffolds provided with a channel ($R_i/R_e = 0.375$) cultured in the perfused bioreactor and under static conditions measured by HPLC. (**B**) Lactate concentration profiles for scaffolds provided with a channel ($R_i/R_e = 0.375$) cultured in the perfused bioreactor and under static conditions measured by HPLC. (**c, d**) Number of cells estimated in the scaffold provided with a channel ($R_i/R_e = 0.375$) cultured in the perfused bioreactor and under static conditions. (**E**) Glucose consumption per million of cells estimated in the cell-populated scaffold provided with a channel ($R_i/R_e = 0.375$) cultured in the perfused bioreactor and under static conditions. (**F**) Lactate production per million of cells estimated in the cell-populated scaffold provided with a channel ($R_i/R_e = 0.375$) cultured in the perfused bioreactor and under static conditions. * p<0.01

than the values specific for chondrocytes (33) and in agreement with previous studies (27).

To assess the glucose consumption and the lactate production rate of the cells, we measured the glucose and the lactate concentration (Fig. 5A, B, respectively) in the cell-populated scaffold provided with the channel ($R_i/R_e = 0.375$) cultured with perfusion and under static conditions. The glucose concentration in the perfused scaffolds decreased from 1 mg/mL ad day 0 to 0.75 mg/mL at day 5 (Fig. 5A, black line), whereas the glucose concentration decreased significantly, from 1 to 0.03 mg/ml at day 5 under static conditions (Fig. 5A, red line). As expected, the lactate concentration showed a specular trend. In fact, the lactate concentration measured in the perfused cell-populated scaffolds slightly increased from 0.00 (day 0) to 0.12 mg/mL (day 5) (Fig. 6B, black line). By contrast, the lactate concentration measured in the static controls was notably higher and reached a value of 0.94 mg/mL (Fig. 6B, red line) at day 5 under static culture conditions. As previously described, we estimated cell proliferation during culture time (Figs. 5C, D) and we calculated both the glucose consumption and lactate production of cells by means of Equations [3] and [4]. The results over 5 days of culture are depicted in Figure 5E, F, respectively. The calculated values for glucose consumption ranged from approximately 5.00 to 6.09 μmol/h·10^6 cells and from approximately 5.00 to 7.33 μmol/h·10^6 cells for the scaffold provided with the channel ($R_i/R_e = 0.375$) cultured in the perfusion bioreactor and under static conditions, respectively, in agreement with previous studies (34). The calculated lactate production was significantly lower (from 1.16 to 2.90 μmol/h·10^6 cells) for cells cultured on the scaffold provided with the channel ($R_i/R_e = 0.375$) in the perfusion bioreactor compared to the

one calculated for cells cultured in static conditions (from 14.00 to 25.18 μmol/h·10^6 cells).

Taken together, these results showed that the fluid could flow both through the channel and, a relatively lower fraction, through the porous scaffold region. In addition, the scaffold provided with the channel allowed oxygen and glucose delivery to cells while enabling a significantly lower retention of lactate with respect to the static culture condition.

The results of the computational fluid dynamics (CFD) are shown in Figure 6. We modeled the culture chamber with 4 different scaffold geometries having different values for R_i/R_e, namely $R_i/R_e = 0.743$, $R_i/R_e = 0.375$ corresponding to the experimental model, $R_i/R_e = 0.185$ and $R_i/R_e = 0.000$, corresponding to the full macroporous scaffold model (Fig. 3C). It is worth noting that with the exception of the full macroporous scaffold $R_i/R_e = 0.000$, in which the highest velocity was localized at the strictions, corresponding to the scaffold pores (115.59 ± 14.47 μm/s), the majority of the flow rate flowed through the scaffold channel because of its low hydrodynamic resistance. The resulting velocity in the channel decreased from 584.59 ± 120.22 μm/s for the scaffold with a ratio $R_i/R_e = 0.185$, 262.31 ± 64.90 μm/s for the scaffold with a ratio $R_i/R_e = 0.375$, to an average velocity of 83.06 ± 34.36 μm/s for the scaffold with the highest $R_i/R_e = 0.743$ ratio. However, an increasing fraction of the total flow rate was able to flow through the porous architecture of the scaffold as the R_i/R_e decreased (Fig. 6A, B).

The predicted hydrodynamic shear stress of the full macroporous scaffold ($R_i/R_e = 0.000$) was localized at the pore walls (2.61 ± 0.54 mPa) and this value was slightly greater than the one predicted in a previous study (median wall shear stress, 1.2 mPa) from our group (7). In the porous section for
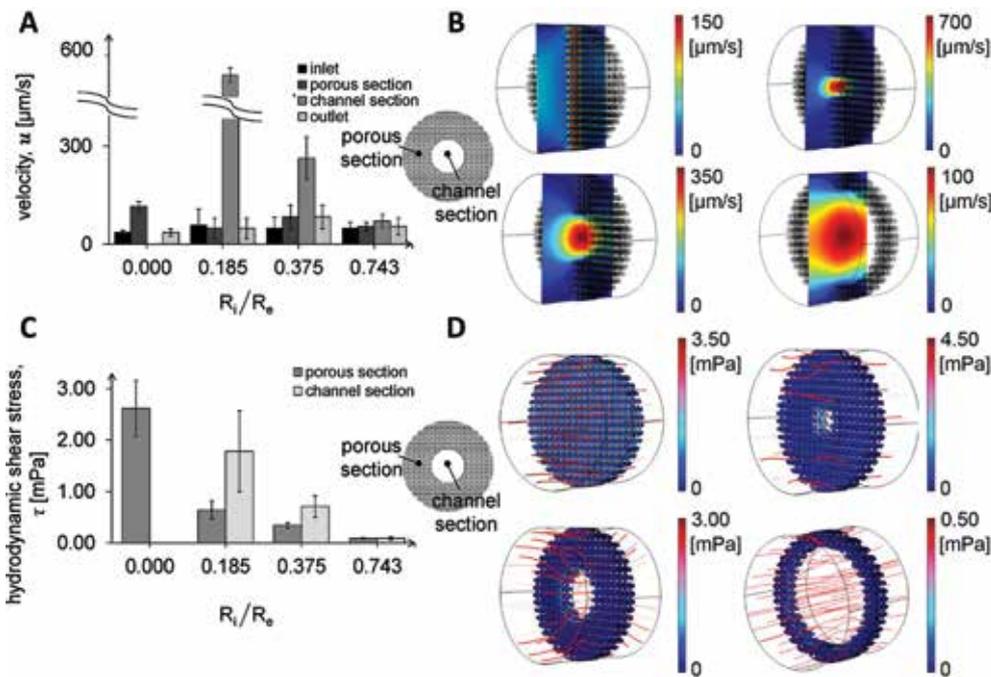
Fig. 6 - Results of the CFD model. (**A**) Predicted average velocity in different areas/section of the model as a function of the R_i/R_e. (**B**) Color map of the velocity magnitude in the culture chamber holding scaffold with decreasing R_i/R_e. (**C**) Predicted hydrodynamic in different areas/section of the model as a function of the R_i/R_e. (**D**) Color map of the predicted hydrodynamic shear stress and fluid velocity streamlines (**in red**) in the culture chamber holding scaffold with decreasing R_i/R_e.

the scaffolds provided with the channel, the viscous stress decreased to 0.64 ± 0.17 mPa, 0.34 ± 0.05 mPa and 0.10 ± 0.01 mPa for the scaffolds with a ratio of $R_i/R_e = 0.185$, 0.375. 0.743, respectively. To assess whether the fluid shear stress negatively affected the cells eventually located close to the scaffold opening (i.e., channel section), we calculated the value and it turned out to be equal to 1.78 ± 0.78 mPa, 0.71 ± 0.21 and 0.09 ± 0.02 mPa for the scaffolds with a ratio of $R_i/R_e = 0.185$, 0.375, 0.743, respectively (Fig. 6C, D).

These findings turned out to be lower than the critical fluid shear stress values affecting cell detachment in 3-D, porous, perfused constructs reported in the literature for cells cultured in a 3-D environment (10, 22, 23). In particular, the CFD results showed that both the hydrodynamic shear stress and velocity decreased as the R_i/R_e of the porous scaffold provided with the channel increased, demonstrating that such a channel can reduce the resistance against the fluid, in particular at a high R_i/R_e, as expected. Moreover, the channel not only prevented shear stress increase and its potential harmful effect on cells (i.e., cell death or detachment), but also diminished the fluid shear stress exerted on cells. Thus, the decrease of low shear stress at short-term and long-term culture can minimize the cell washout, preserve the number of viable cells, and positively affect the homogeneity of the seeded cells on the scaffold to help functional tissue development and maturation (18-21).

To assess whether the porous part of the scaffold provided with the channel can take advantage of the direct exposure to a fraction of the culture medium and therefore to the convective nutrient transport, we illustrated the fluid flow by means of streamlines. It turned out that streamlines may easily penetrate the porous scaffold (Fig. 7B). In addition, we coupled the fluid dynamics to the oxygen and glucose transport modeled by the convection-diffusion-reaction equations (Eqs. 9-11). The predicted oxygen concentration at the outlet $c_{O_{2OUT}}$ of the

full macroporous scaffold ($R_i/R_e = 0.000$) was 0.02 ± 0.004 mol/m³, meaning a hypoxic cell condition. The oxygen tension increased up to 0.12 ± 0.04 mol/m³, 0.14 ± 0.05 mol/m³ and 0.17 ± 0.03 mol/m³ for the scaffolds provided with the channel, with a ratio of $R_i/R_e = 0.185$, 0.375, 0.743, respectively (Figs. 7A, B). Concerning the glucose concentration, at the outlet of the culture chamber $c_{Glu_{OUT}}$, we predicted a value of 1.01 ± 0.20 mol/m³ for the full macroporous scaffold ($R_i/R_e = 0.000$). The glucose concentration at the outlet was 2.27 ± 1.79 mol/m³, 3.86 ± 1.60 mol/m³ and 4.85 ± 0.74 mol/m³ for the scaffolds provided with the channel, with a corresponding ratio of $R_i/R_e = 0.185$, 0.375, 0.743, (Fig. 7C, D).

We observed a difference of approximately 12.04% and 12.98% between the experimental measurements and numerical predictions for the scaffold provided with the channel, with $R_i/R_e = 0.375$ for both the oxygen and glucose tension, respectively. These differences were due most likely to the assumptions in the numerical model. In particular, we assumed a 1-μm-thick homogeneous cell monolayer all over the macroporous scaffold surface area, thus overestimating the reaction (i.e., oxygen and glucose consumption) terms in Equations [10] and [11], as well as the relevant predicted concentration species. A further simplification consisted in neglecting the cell as well as the ECM growth, which will be a topic of further investigation in future work. The tissue growth process depends on biochemical and biophysical variables varying both in space and time, therefore an essential step toward the development of functional tissues is to precisely model the dual/mutual interaction between the bioreactor microenvironment and the cell-matrix dynamics (1, 28). However, the perfused bioreactor employed in this study belongs to the first-generation of bioreactors (i.e., macroscopic devices hosting cell-populated constructs of several mm in dimensions) in which the global culture parameters can be experimentally measured on the construct by means of classical destructive
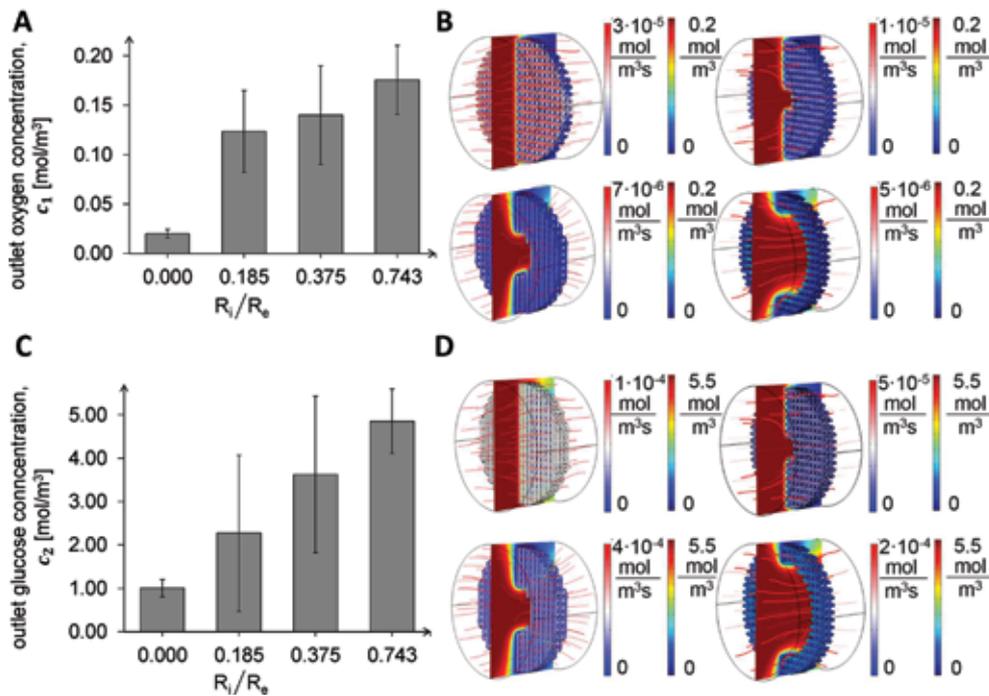
Fig. 7 - Results of the CFD coupled to the mass transport model. (**A**) Predicted outlet oxygen concentration as a function of the R_i/R_e. (**B**) Color map of the oxygen concentration and of the oxygen consumption rate in the culture chamber holding scaffolds with decreasing R_i/R_e. (**C**) Predicted outlet glucose concentration as a function of the R_i/R_e. (**D**) Color map of the glucose concentration and of the glucose consumption rate in the culture chamber holding scaffolds with decreasing R_i/R_e.

assays (Fig. 4E-G) or directly measured at the inlet and outlet channels (Figs. 4A-D and 5). Thus, as it was conceived, the cell construct was not experimentally accessible and did not allow assessment of the evolution of cell/matrix growth at different time points during culture unless done destructively.

Despite these limitations, cells cultured in such macroporous scaffolds provided with a channel may offer several advantages; i) they are exposed directly to flow, ii) they do not experience harmful viscous stresses, iii) they are delivered nutrients by convection, all of this without the need of a hollow fiber. Taken together, these results allowed us to demonstrate that the macroporous scaffold provided with a channel can be considered the equivalent of a hollow fiber integrated into a porous scaffold without the need of a physical fiber. Unless a physical barrier is needed for the separation of compartments, our results imply several technical and practical advantages, including the fabrication, characterization, and integration of fibers within a macroporous scaffold (3). In addition, our findings showed that the macroporous scaffold can be used as a "reference domain" for a systematic investigation of culture parameters in perfused bioreactors for large-size constructs, including hollow fiber-integrated bioreactors, and as a reliable experimental device for an in silico evaluation of scaffold designs.

Conclusions

We developed an experimental-numerical investigation on the effects of the macroporous scaffold geometry on cell culture parameters. In particular, the experimental model consisted of a perfused bioreactor to culture a macroporous scaffold provided with a channel in its center. We also developed a numerical model in the aim to further describe the contribution of the geometry of such a scaffold on fluid dynamics and nutrient transport (i.e., oxygen and glucose).

The experimental findings showed that our bioreactor allowed several crucial parameters to be easily assessed. Coupling these experimental results with the numerical model we were able to predict both fluid dynamics (i.e., the velocity field and the viscous stress, which would be practically impossible to measure) and mass transport variables in a good agreement with the experimental measurements and the literature.

The computational results showed that both the hydrodynamic shear stress and velocity decreased as the ratio increased, confirming that the reduction of the resistance against a fluid flow can be employed as a potential strategy for low scaffold porosity caused by cell growth and matrix secretion. The scaffold not only prevented the increase of shear stress exerted on cells but allowed them to be exposed to low and not harmful values. We demonstrated that cells cultured in these macroporous scaffolds provided with a channel may offer several advantages; i) they are exposed directly to flow, ii) they do not experience harmful viscous stresses, iii) they are delivered nutrients by convection without the need of a hollow fiber. In conclusion, our macroporous scaffold with a channel can be interpreted as a simplified "representative/reference unit" for the systematic study of both perfused culture systems and hollow fiber-integrated scaffolds for large-scale tissue engineering, overcoming their technological and practical limitations.

References

1. Nava MM, Raimondi MT, Pietrabissa R. A multiphysics 3D model of tissue growth under interstitial perfusion in a tissue-engineering bioreactor. Biomech Model Mechanobiol. 2013;12(6):1169-1179.
2. Gauvin R, Guillemette M, Dokmeci M, Khademhosseini A. Application of microtechnologies for the vascularization of engineered tissues. Vasc Cell. 2011;3(1):24.
3. Eghbali H, Nava MM, Mohebbi-Kalhori D, Raimondi MT. Hollow fiber bioreactor technology for tissue engineering applications. Int J Artif Organs. 2016;39(1):1-15.
4. Grayson WL, Bhumiratana S, Cannizzaro C, et al. Effects of initial seeding density and fluid perfusion rate on formation of tissue-engineered bone. Tissue Eng Part A. 2008;14(11):1809-1820.
5. Rouwkema J, Rivron NC, van Blitterswijk CA. Vascularization in tissue engineering. Trends Biotechnol. 2008;26(8):434-441.
6. Hoo SP, Loh QL, Yue Z, et al. Preparation of a soft and interconnected macroporous hydroxypropyl cellulose methacrylate scaffold for adipose tissue engineering. J Mater Chem B. 2013;1(24):3107-3117.
7. Raimondi MT, Candiani G, Cabras M, et al. Engineered cartilage constructs subject to very low regimens of interstitial perfusion. Biorheology. 2008;45(3-4):471-478.
8. Domingos M, Dinucci D, Cometa S, Alderighi M, Bártolo PJ, Chiellini F. Polycaprolactone Scaffolds Fabricated via Bioextrusion for Tissue Engineering Applications. Int J Biomater. 2009;Sep 8. doi: 10.1155/2009/239643. [Epub ahead of print].
9. Laganà M, Raimondi MT. A miniaturized, optically accessible bioreactor for systematic 3D tissue engineering research. Biomed Microdevices. 2012;14(1):225-234.
10. McCoy RJ, OBrien FJ. Influence of shear stress in perfusion bioreactor cultures for the development of three-dimensional bone tissue constructs: a review. Tissue Eng Part B Rev. 2010;16(6):587-601.
11. Freyria AM, Yang Y, Chajra H, et al. Optimization of dynamic culture conditions: effects on biosynthetic activities of chondrocytes grown in collagen sponges. Tissue Eng. 2005;11(5-6):674-684.
12. Viswanathan P, Ondeck MG, Chirasatitsin S, et al. 3D surface topology guides stem cell adhesion and differentiation. Biomaterials. 2015;52:140-147.
13. Fusco S, Panzetta V, Embrione V, Netti PA. Crosstalk between focal adhesions and material mechanical properties governs cell mechanics and functions. Acta Biomater. 2015;23:63-71.
14. Jaatinen L, Young E, Hyttinen J, Vörös J, Zambelli T, Demkó L. Quantifying the effect of electric current on cell adhesion studied by single-cell force spectroscopy. Biointerphases. 2016;11(1):011004.
15. Hong MH, Kim YH, Ganbat D, Kim DG, Bae CS, Oh DS. Capillary action: enrichment of retention and habitation of cells via micro-channeled scaffolds for massive bone defect regeneration. J Mater Sci Mater Med. 2014;25(8):1991-2001.
16. Bettahalli NM, Vicente J, Moroni L, et al. Integration of hollow fiber membranes improves nutrient supply in three-dimensional tissue constructs. Acta Biomater. 2011;7(9):3312-3324.
17. Hadjizadeh A, Mohebbi-Kalhori D. Porous hollow membrane sheet for tissue engineering applications. J Biomed Mater Res A. 2010;93(3):1140-1150.
18. Li W, Li M, Chen Y, Zhang S, Qi N. Various seeding methods for tissue development of human umbilical-cord-derived mesenchymal stem cells in 3-dimensional PET matrix. Biotechnol Bioprocess Eng. 2014;19(1):108-117.
19. Leferink AM, Hendrikson WJ, Rouwkema J, Karperien M, van Blitterswijk CA, Moroni L. Increased cell seeding efficiency in bioplotted three-dimensional PEOT/PBT scaffolds. J Tissue Eng Regen Med. 2016;10(8):679-689.
20. Holy CE, Shoichet MS, Davies JE. Engineering three-dimensional bone tissue in vitro using biodegradable scaffolds: investigating initial cell-seeding density and culture period. J Biomed Mater Res. 2000;51(3):376-382.
21. Talukdar S, Nguyen QT, Chen AC, Sah RL, Kundu SC. Effect of initial cell seeding density on 3D-engineered silk fibroin scaffolds for articular cartilage tissue engineering. Biomaterials. 2011;32(34):8927-8937.
22. Provin C, Takano K, Sakai Y, Fujii T, Shirakashi R. A method for the design of 3D scaffolds for high-density cell attachment and determination of optimum perfusion culture conditions. J Biomech. 2008;41(7):1436-1449.
23. Sinlapabodin S, Amornsudthiwat P, Damrongsakkul S, Kanokpanont S. An axial distribution of seeding, proliferation, and osteogenic differentiation of MC3T3-E1 cells and rat bone marrow-derived mesenchymal stem cells across a 3D Thai silk fibroin/gelatin/hydroxyapatite scaffold in a perfusion bioreactor. Mater Sci Eng C Mater Biol Appl. 2016;58:960-970.
24. Plunkett NA, Partap S, OBrien FJ. Osteoblast response to rest periods during bioreactor culture of collagen-glycosaminoglycan scaffolds. Tissue Eng Part A. 2010;16(3):943-951.
25. Domingos M, Chiellini F, Gloria A, Ambrosio L, Bartolo P, Chiellini E. Effect of process parameters on the morphological and mechanical properties of 3D Bioextruded poly (ε-caprolactone) scaffolds. Rapid Prototyp J. 2012;18(1):56-67.
26. Tschiersch H, Stangelmayer A, Liebsch G, Rolletschek H, Borisjuk L. Planar oxygen sensors for non invasive imaging in experimental biology. INTECH Open Access Publisher; 2011.
27. Raimondi MT, Giordano C, Pietrabissa R. Oxygen measurement in interstitially perfused cellularized constructs cultured in a miniaturized bioreactor. J Appl Biomater Funct Mater. 2015;13(4):e313-e319.
28. Guyot Y, Luyten FP, Schrooten J, Papantoniou I, Geris L. A three-dimensional computational fluid dynamics model of shear stress distribution during neotissue growth in a perfusion bioreactor. Biotechnol Bioeng. 2015;112(12):2591-2600.
29. Marín-Hernández A, López-Ramírez SY, Del Mazo-Monsalvo I, et al. Modeling cancer glycolysis under hypoglycemia, and the role played by the differential expression of glycolytic isoforms. FEBS J. 2014;281(15):3325-3345.
30. Comsol Multiphysics users' guide 2015, Burlington, MA, USA.
31. Davisson T, Sah RL, Ratcliffe A. Perfusion increases cell content and matrix synthesis in chondrocyte three-dimensional cultures. Tissue Eng. 2002;8(5):807-816.
32. Raimondi MT, Moretti M, Cioffi M, et al. The effect of hydrodynamic shear on 3D engineered chondrocyte systems subject to direct perfusion. Biorheology. 2006;43(3-4):215-222.
33. Zhou S, Cui Z, Urban JP. Nutrient gradients in engineered cartilage: metabolic kinetics measurement and mass transfer modeling. Biotechnol Bioeng. 2008;101(2):408-421.
34. Khademi R, Mohebbi-Kalhori D, Hadjizadeh A. Computational study of culture conditions and nutrient supply in a hollow membrane sheet bioreactor for large-scale bone tissue engineering. J Artif Organs. 2014;17(1):69-80.